Author(s): Henning, Greg; Khoo, T. L.; Lopez-Martens, A.; Seweryniak, D.; Alcorta, M.; Asai, M.; Back, B. B.; Bertone, P. F.; Boilley, D.; Carpenter, P.; Chiara, C. J.; Chowdhury, P.; Gall, B.; Greenlees, Paul; Gürdal, G.; Hauschild, K.; Heinz, A.; Hoffman, C. R.; Janssens, R. V. F.; Karpov, A. V.; Kay, B. P.; Kondev, F. G.; Lakshmi, S.; Lauritsen, T.; Lister, C. J.; McCutchan, E. A.; Nair, C.; Piot, J.; Potterveld, D.; Reiter, P.; Rogers, A. M.; Rowley, N.; Zhu, S.

Title: Fission Barrier of Superheavy Nuclei and Persistence of Shell Effects at High Spin: Cases of 254No and 220Th

Year: 2014

Version:

Please cite the original version:

Henning, G., Khoo, T. L., Lopez-Martens, A., Seweryniak, D., Alcorta, M., Asai, M., Back, B.B., Bertone, P. F., Boilley, D., Carpenter, P., Chiara, C. J., Chowdhury, P., Gall, B., Greenlees, P., Gürdal, G., Hauschild, K., Heinz, A., Hoffman, C. R., Janssens, R. V. F., . . . Zhu, S. (2014). Fission Barrier of Superheavy Nuclei and Persistence of Shell Effects at High Spin: Cases of 254No and 220Th. Physical Review Letters, 113(26), Article 262505. https://doi.org/10.1103/PhysRevLett.113.262505

Fission Barrier of Superheavy Nuclei and Persistence of Shell Effects at High Spin: Cases of ^{254}No and ^{220}Th

Greg Henning,[1,2,*] T. L. Khoo,[2] A. Lopez-Martens,[1] D. Seweryniak,[2] M. Alcorta,[2] M. Asai,[3] B. B. Back,[2] P. F. Bertone,[2,†] D. Boilley,[4,5] M. P. Carpenter,[2] C. J. Chiara,[2,6] P. Chowdhury,[7] B. Gall,[8,9] P. T. Greenlees,[10] G. Gürdal,[11,2] K. Hauschild,[1] A. Heinz,[12,13] C. R. Hoffman,[2] R. V. F. Janssens,[2] A. V. Karpov,[14] B. P. Kay,[2] F. G. Kondev,[2] S. Lakshmi,[7] T. Lauritsen,[2] C. J. Lister,[7] E. A. McCutchan,[2] C. Nair,[2] J. Piot,[8,9] D. Potterveld,[2] P. Reiter,[15] A. M. Rogers,[2] N. Rowley,[16] and S. Zhu[2]

[1]*CSNSM, IN2P3-CNRS, and Université Paris Sud, Bat. 104-108, F-91405 Orsay, France*
[2]*Argonne National Laboratory, Argonne, Illinois 60439, USA*
[3]*Advanced Science Research Center, Japan Atomic Energy Research Institute, Tokai, Ibaraki 319-1195, Japan*
[4]*GANIL, CEA-DSM, and IN2P3-CNRS, B.P. 55027, F-14076 Caen Cedex, France*
[5]*Université de Caen Basse-Normandie, F-14032 Caen Cedex, France*
[6]*University of Maryland, College Park, Maryland 20742, USA*
[7]*University of Massachusetts Lowell, Lowell, Massachusetts 01854, USA*
[8]*Université de Strasbourg, IPHC, 23 rue du Loess, 67037 Strasbourg, France*
[9]*CNRS, UMR7178, 67037 Strasbourg, France*
[10]*Department of Physics, University of Jyväskylä, FI-40014 Jyväskylä, Finland*
[11]*DePaul University, Chicago, Illinois 60604, USA*
[12]*Fundamental Fysik, Chalmers Tekniska Hogskola, 412 96 Göteborg, Sweden*
[13]*WNSL, Yale University, New Haven, Connecticut 06511, USA*
[14]*Flerov Laboratory of Nuclear Reactions, JINR, Dubna, 141980, Russia*
[15]*Institut für Kernphysik, Universität zu Köln, D-50937 Köln, Germany*
[16]*IPN, CNRS/IN2P3, Université Paris-Sud 11, F-91406 Orsay Cedex, France*

(Received 8 September 2014; published 30 December 2014)

We report on the first measurement of the fission barrier height in a heavy shell-stabilized nucleus. The fission barrier height of ^{254}No is measured to be $B_f = 6.0 \pm 0.5$ MeV at spin $15\hbar$ and, by extrapolation, $B_f = 6.6 \pm 0.9$ MeV at spin $0\hbar$. This information is deduced from the measured distribution of entry points in the excitation energy versus spin plane. The same measurement is performed for ^{220}Th and only a lower limit of the fission barrier height can be determined: $B_f(I) > 8$ MeV. Comparisons with theoretical fission barriers test theories that predict properties of superheavy elements.

DOI: 10.1103/PhysRevLett.113.262505 PACS numbers: 27.90.+b, 21.10.Hw, 24.60.Dr, 24.75.+i

Superheavy elements (SHE) owe their existence to quantum shell effects, which create a sizable barrier against fission. Without such shell-stabilizing effects, i.e., with only the liquid-drop component, the fission barrier in a heavy nuclide such as $^{254}_{102}$No would be small, 0.9 MeV [1,2], and the spontaneous fission lifetime of ^{254}No would be 13 orders of magnitude shorter than observed [3]. The height of the fission barrier (defined as the energy difference of the ground and saddle states) determines the stability of the SHE against fission and is one factor affecting its production cross section. SHE are generally produced in fusion-evaporation reactions. As the hot compound nucleus cools by neutron emission, its survival against fission is governed by the barrier height. In fact, the high fission barriers predicted around $Z = 114$ and $N = 184$ [4] are thought to be responsible for reversing at $Z = 112$ the trend of decreasing evaporation-residue cross sections as a function of atomic number Z, resulting in a maximum effect at $Z = 114$–115 [5]. (Other factors could also play a role in decreasing the fission probability [6].)

Clearly, a determination of the fission barrier is an important goal for experiment. Measurements to study SHE are challenging as the production rates can be as low as a few nuclei per month. The cross sections to produce deformed transfermium nuclei, which are stabilized by the same shell energy, are larger and studies of fission barrier properties become possible. ^{254}No is the best candidate for such a study as it has the highest cross section (although still small at around 1 μb) of the heaviest nuclei and the structure of its excited states is quite well known [7–15]. A previous attempt at determining the height of its fission barrier yielded a lower limit of ~5 MeV for spins up to $22\hbar$ [16], which did not allow for differentiating between the available theoretical predictions. Indeed, density functional theory (DFT) calculations based on the Gogny D1S and Skyrme interactions give a barrier height between 6 and 12.6 MeV [17–21]. Calculations based on the macroscopic-microscopic model give a lower value of 6.8 MeV [4,22]. In this Letter, we present the first measurement of the barrier height B_f for ^{254}No, which becomes the heaviest nuclide for which the barrier has been measured, the previous being

$^{249}_{97}$Bk [23]. Furthermore, a comparison with $^{220}_{90}$Th, with 12 fewer protons, highlights the role of shell effects.

The fission barrier can be deduced by measuring the fission probability $P_{\text{fission}}(E^{\star})$ as a function of excitation energy, as first exploited following transfer reactions [24]. Such reactions are not possible for nuclei with $Z > 98$, as there is no target to enable fission excitation function measurements by (n, f) or (d, pf) reactions, for example. However, below the neutron threshold, one can exploit the fact that $P_{\text{fission}} = 1 - P_{\gamma}$. The fission width Γ_{fission} rapidly dominates the γ-decay width Γ_{γ} near and above the saddle energy E_{saddle}, resulting in a sharp drop of P_{γ} in a narrow interval ($\approx$0.5 MeV). (This has been demonstrated by our analytical calculations [25,26] of the γ and fission widths.) Therefore, a measurement of P_{γ} allows a clear determination of the saddle position—as long as E_{saddle} is below the neutron separation energy S_n. As pointed out in Ref. [16], one can use the entry distribution—i.e., the distribution in excitation energy versus spin $(E^{\star}, I)$ of starting points for γ decay to the ground state—to determine the γ-decay probability P_{γ} and, thereby, the saddle energy.

We populated ^{254}No with the reaction ^{208}Pb(^{48}Ca, $2n$) at two beam energies: 219 and 223 MeV (217 and 220.5 MeV at the center of the target). ^{220}Th was studied with the reaction ^{176}Yb(^{48}Ca, $4n$), with a beam energy of 219 MeV (215.7 MeV at the center of the target). The $\sim$10 pnA ^{48}Ca beam was delivered by the superconducting linear accelerator ATLAS at Argonne National Laboratory and impinged on a $\sim$0.5 mg/cm^2-thick rotating ^{208}Pb target. The current was intentionally limited to avoid saturating the γ-ray detectors with fission-fragment γ rays. The stationary ^{176}Yb target for production of ^{220}Th was 0.9 mg/cm^2 thick. The γ-ray detector array Gammasphere [27] was used to perform calorimetric measurements at the target position, as well as high-resolution γ-ray spectroscopy. In calorimetric measurements, both the germanium detectors and the bismuth germanate (BGO) Compton suppression shields are used to measure the sum energy and multiplicity of the γ rays. The evaporation residues were separated from the scattered beam by the fragment mass analyzer (FMA) [28] and dispersed according to their mass-to-charge ratio. At the focal plane of the FMA, evaporation residues were detected in a parallel grid avalanche counter (PGAC), which measured the energy loss and the x and y positions of the recoils (z being along the beam direction). Finally, the evaporation residues were implanted in a 64×64 mm^2 double-sided silicon strip detector (DSSD) with 160 orthogonal strips on each side, allowing the detection of the energy and position of implanted recoils and of the α or electron decays occurring inside a given DSSD pixel.

The recoils were fully identified at the focal plane of the FMA by a combination of gates on the implantation energy in the DSSD, the time of flight between the PGAC and the DSSD, the x position at the dispersive plane, and the energy loss in the PGAC. The number of observed ^{254}No events at each beam energy (915 events during 43 hours for $E_{\text{Beam}} = 219$ MeV and 1475 events during 118 hours for $E_{\text{Beam}} = 223$ MeV) is consistent with the known cross sections [29–31] and the expected transmission of the FMA for this reaction ($\approx$7%).

The total energy released and the multiplicity of γ rays emitted in each reaction were determined from the sum energy and the number of hits in the Gammasphere modules (each defined as a Ge detector and its surrounding BGO shield). The detector response and efficiency are taken into account by a Monte Carlo unfolding procedure [32], using the energy and multiplicity responses, which were measured with an ^{88}Y source [33,34]. The experimental distributions were unfolded many times, with different random seeds. Each set of results was analyzed individually to separate real and reproducible features from fluctuations of the Monte Carlo process (see Ref. [34] for details). The results reported below represent the average from this process and the uncertainties reflect both the scatter and data uncertainty. The contribution of neutron signals in Gammasphere was simulated with the GEANT4 [35,36] code and found to be negligible.

The deduced multiplicity M was transformed into a spin value using the expression

$$I = \Delta I(M - N_{\text{stat}}) + \Delta I_{\text{stat}} N_{\text{stat}} + I_{\text{CE}}, \qquad (1)$$

where ΔI is the average spin carried by a γ transition between nuclear levels, N_{stat} is the average number of statistical γ rays, ΔI_{stat} is the average spin carried by a statistical γ ray and I_{CE} is the average spin removed by internal conversion electrons. The deduced sum energy is transformed into the total excitation energy $E^{\star} = E_{\text{sum}\gamma} + E_{\text{CE}}$, where E_{CE} is the average energy removed by the conversion electrons. The values of the parameters in these equations are determined from experimental data and the properties of the known level scheme [7–13] and are given in Table I. These parameters are for the average decays in the nucleus. The uncertainty on these parameters leads to $\approx 2\hbar$ uncertainty on the final spin values.

TABLE I. Parameters used for the multiplicity-to-spin conversion and total excitation energy determination. These have been calculated or extracted from the published level schemes [7–11,14,15,37], experimental spectra (Refs. [12,13] and the present data). The conversion electron contribution is calculated for the K and the L, M, N electron shells separately to account for the high fluorescence yield of K shells and the detection of K x rays.

	$\Delta I(\hbar/\gamma)$	N_{stat}	$\Delta I_{\text{stat}}(\hbar/\gamma)$	$I_{\text{CE}}(\hbar)$	E_{CE} (keV)
^{254}No	2	3	0.25	8.8	860
^{220}Th	1.5	4	0.25	0.7	110

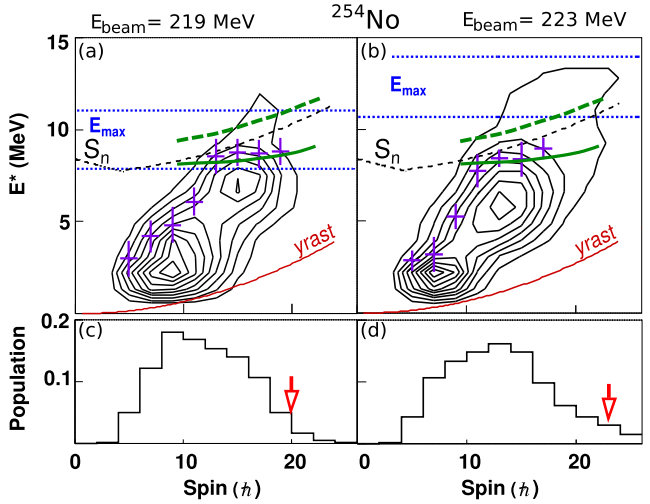

FIG. 1 (color online). Entry distributions for $E_{\mathrm{beam}} = 219$ (a) and 223 MeV (b) obtained from one unfolding procedure. Each contour line corresponds to a decrement of 10% of the maximum population. The yrast line and neutron separation energy are represented by the solid red and dotted black lines, respectively. The neutron separation energy at spin I is defined as $S_n(I) = S_n + E^{A-1}_{\mathrm{yrast}}(I + 1/2) - E^{A}_{\mathrm{yrast}}(I)$, where S_n is the ground-state mass difference, for $I > I^{A-1}_{\mathrm{g.s}}$, and linearly extrapolated to the energy of the first $I = 1/2\hbar$ state for $I < I^{A-1}_{\mathrm{g.s}}$. The maximum possible excitation-energy range is represented by the blue dotted lines, with the higher (lower) value corresponding to a reaction at the front (back) of the target. The half-maximum point for each spin slice is marked in purple with error bars. The solid and dashed green lines between 10 and $22\hbar$ represent the $E_{1/2}$ values predicted with our deduced value for B_f and with B_f 2 MeV higher. Panels (c) and (d) show the corresponding spin projections of the distributions. The points where the spin distributions fall to 10% of their maximum are marked with a red arrow.

Figure 1 provides the entry distributions for ^{254}No measured at the two beam energies. At the highest spins and energies, there is a contribution from random summing, where a ^{254}No cascade sums with one from fission. For $E^{\star} < 6$ MeV and $I < 11\hbar$, the events do not represent the true entry distribution since they include displaced events, which originate from γ cascades feeding isomers [9–11,14,15], whose decays occur outside Gammasphere. This leads to a shift towards low energy and spin for a fraction of the distribution, but does not compromise the high-energy and high-spin survival information from the upper part of the distribution. (The isomer events represent ~30% of the ^{254}No population.)

The entry distribution was analyzed by examining the energy distribution corresponding to each $2\hbar$–wide spin bin in order to determine the energy $E_{1/2}$, where the distribution falls to 50% of the maximum value (purple crosses in Fig. 1). At the 219 MeV beam energy, limitations on $E_{1/2}$ are imposed partially by the maximum allowable energy in ^{254}No, indicated by the horizontal dashed lines in Figs. 1(a) and 1(b), corresponding to zero kinetic energy for the two evaporated neutrons. At 223 MeV, this limitation is no longer a factor, allowing the role of fission to be clearly visible. For I between 13 and $17\hbar$, there is no increase of $E_{1/2}$ [see Figs. 1(a) and 1(b)] when the beam energy increases; i.e., a saturation of $E_{1/2}$ is observed. The saturation occurs even though higher energy states are favored due to higher level densities. The termination of γ decay must be due to the rapid onset of fission near the top of the fission barrier. In this manner, the data directly reveal where fission sets in and overwhelms γ decay. This point is illustrated in Fig. 1, where the green dashed line indicates that $E_{1/2}$ would have been significantly higher if B_f were artificially increased to 8.5 MeV (i.e., 0.8 MeV above S_n); in this case, the termination of γ decay is caused by neutron evaporation. When the experimentally deduced B_f is used in the calculation, the computed (full green line) and experimental $E_{1/2}$ values are in agreement.

One expects $E_{1/2}$ to be near E_{saddle}. Indeed, our statistical decay calculations, using the KEWPIE2 and NRV codes [38,39], have shown that the difference

$$\Delta = E_{1/2} - E_{\mathrm{saddle}} \tag{2}$$

decreases from ≈1 MeV at $I = 0\hbar$ to 0.3 MeV at $I = 17\hbar$. From the decay calculations, we extract $\Delta(I) = 1(0.15) - I \times 0.04(0.02)$ MeV. (These calculations account for the fusion-evaporation reaction process, the population profile after neutron evaporation, and the effect of γ and fission competition). After a correction given by Eq. (2), one is able to determine E_{saddle} from the $E_{1/2}$ value extracted from the experimental energy distribution at a given spin. Figure 2 plots the deduced E_{saddle} versus spin. The energy of the saddle above the yrast line defines the fission barrier at each spin. One sees that the fission barrier diminishes with spin, as the yrast and saddle states converge due to the difference in deformation and moments of inertia [40].

The measurement gives E_{saddle} growing from 6.5 ± 1 MeV at spin $11\hbar$ to 7.9 ± 0.5 MeV for $I = 17\hbar$. Assuming a rotorlike spin dependence of the saddle energy as $E_{\mathrm{saddle}} = B_f(0) + (I(I+1)/2\mathcal{J}_{\mathrm{saddle}})$, we extract a moment of inertia $\mathcal{J}_{\mathrm{saddle}} = 125 \pm 60\hbar^2/$ MeV and B_f values of 6.0 ± 0.5 and 6.6 ± 0.9 MeV at spins 15 and 0, respectively (the latter by extrapolation). Our results concur with the previous experimental lower bounds [16]. The spin dependence given by $\mathcal{J}_{\mathrm{saddle}}$ is similar to the value ($140\hbar^2/$ MeV) from DFT with the Gogny D1S interaction [17]. However, this method gives a larger $B_f(0)$ of 8.7 MeV than our value of 6.6 ± 0.9 MeV. Another calculation [18] with the same Gogny D1S interaction obtains a barrier of 6.9 or 6.1 MeV. However, that is for a dynamical barrier appropriate for spontaneous fission with tunneling via the least-action path, whereas our measurement gives the static barrier, which governs the fission threshold. DFT calculations [19,20] with Skyrme interactions yield significantly

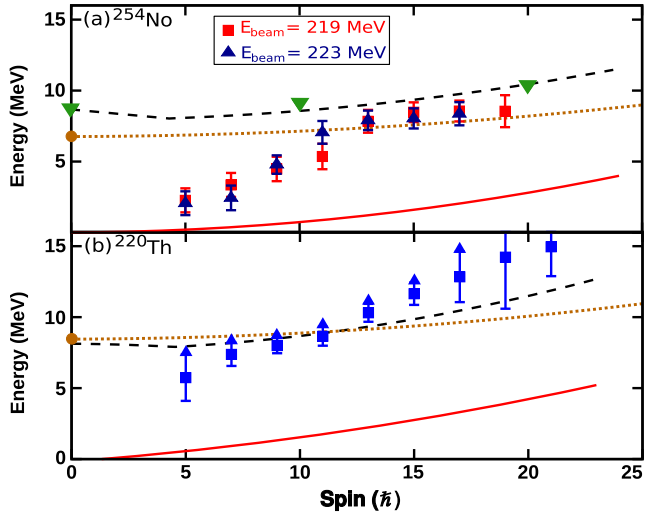

FIG. 2 (color online). Plot of the E_{saddle} points extracted from the entry distributions of ^{254}No (a) and ^{220}Th (b). For ^{254}No, points are given for the two beam energies: 219 (red squares) and 223 MeV (blue triangles). For ^{220}Th, the blue squares are the lower limits for E_{saddle}—see the text. The red line is the yrast energy; the dashed black line is the neutron separation energy. Theoretical saddle energies are shown for comparison: the triangles are from DFT [17]; the circles are from a macroscopic-microscopic model [4]. Based on the latter, the dotted brown line shows our estimate of saddle energies at high spin—see the text.

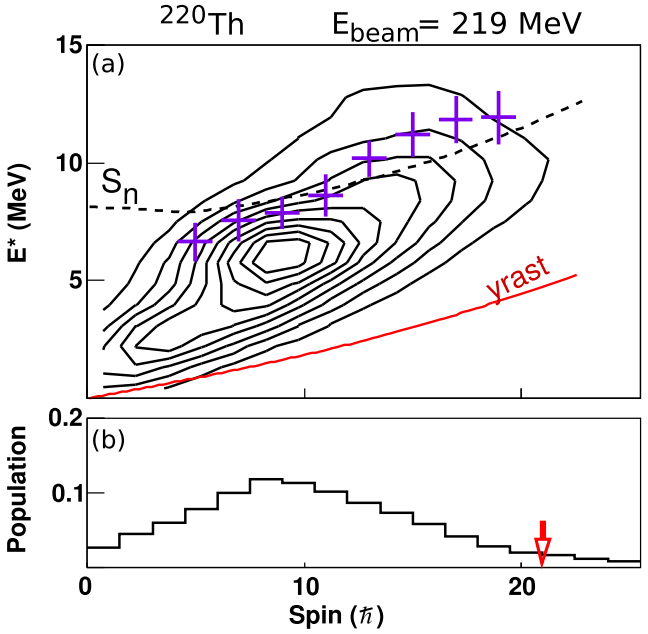

FIG. 3 (color online). Entry distribution for ^{220}Th, with its spin projection. See Fig. 1 for a description.

higher barriers (9.6 and 8.6 or 12.5 MeV, respectively). In contrast, the macroscopic-microscopic prediction of 6.8 MeV [4,22] is in agreement with experiment. With this model, no saddle energies at high spin have been reported; we have estimated them using a liquid-drop moment of inertia for the calculated [4,41] deformation parameters of the saddle shape—see the dotted lines in Fig. 2.

A similar analysis was performed for ^{220}Th, using the parameters in Table I. The extracted entry distribution (Fig. 3) matches that obtained in a previous measurement [42]. The entry distribution in Fig. 3(a) and the $E_{1/2}$ values (purple crosses) from projections of individual spin slices extend beyond the line denoting the neutron separation energy. This indicates that the fission barrier has to be above (or close to) the neutron separation energy. Hence, neutron emission competes with fission and γ decay in ^{220}Th. As a consequence, $E_{1/2}$ is governed not only by B_f, but also by S_n, making it not possible to cleanly deduce B_f as for ^{254}No. Nevertheless, for ^{220}Th, the $E_{1/2}$ values set a lower bound on E_{saddle}, which is plotted in Fig. 2(b): for I between 11 and 21$\hbar$, we find $B_f(I) > 8$ MeV. This also implies $B_f(0) > 8$ MeV, consistent with the prediction (8.45 MeV) of the macroscopic-microscopic model [4]. The saddle energies at high spin based on this model are estimated in the same manner as for ^{254}No, and are indicated in Fig. 2(b). Those estimated values of E_{saddle} are compatible with the extracted lower bounds for spin $I = 11$–$21\hbar$.

The extracted fission barriers at spin 15$\hbar$ in ^{254}No and ^{220}Th are $B_f(15) = 6.0$ and > 8 MeV. Despite the atomic number of ^{254}No being larger by 12, its fission barrier is rather similar to that of ^{220}Th because the former has a significantly larger microscopic energy (comprised of shell, deformation, and pairing energies): 5.2 versus > 3 MeV. A common practice [3] for estimating the fission barrier is to add the ground-state microscopic energy (3.97 and 1.62 MeV for ^{254}No and ^{220}Th, [43,44]) to the liquid-drop barrier (0.9 and 5.4 MeV, from the program BARFIT [1,2]), which is tantamount to assuming that there is no microscopic correction at the saddle. This method would yield barriers of 4.9 and 7.0 MeV for the ground states of ^{254}No and ^{220}Th. A more sophisticated calculation based on the microscopic-macroscopic model yields larger barriers of 6.8 and 8.5 MeV [4], closer to the experimentally deduced barrier heights. The larger theoretical and experimental barriers suggest a positive (1.7 ± 0.9 MeV) microscopic effect at the saddle, which is quite prevalent for $Z = 90$–96, as noted in Ref. [45]. Our measurement for ^{254}No indicates the trend persists to $Z = 102$.

The maximum spins I_{max} for ^{254}No and ^{220}Th are 17 (Ref. [16]), 20, and 23$\hbar$ (for $E_{beam} = 215$, 219, and 223 MeV) and 20 (Ref. [42]) and 21$\hbar$ (for $E_{beam} = 206$ and 219 MeV). For ^{254}No, there is a steady increase in I_{max} with small increments in the beam energy. In contrast, for ^{220}Th, I_{max} hardly grows at two very different beam energies, indicating that a limit has been reached for the maximum angular momentum it can sustain. Unexpectedly,

I_{max} for ^{254}No at the 223 MeV beam energy is larger than for ^{220}Th, even though the former has a smaller fission barrier. Two factors account for this observation. First, B_f decreases more rapidly with spin in ^{220}Th due to the larger difference between the yrast and saddle deformations [40]. This effect is accentuated by the formation process, where for ^{220}Th there are four (versus two for ^{254}No) steps of neutron or fission competition, which decrease the survival probability of the higher partial waves. In all cases, coupled-channel calculations indicate considerably larger I_{max} in the entrance channel, e.g., up to $\sim 55\hbar$ for ^{254}No at 223 MeV. However, as the compound nucleus cools by neutron evaporation, the highest partial waves do not survive the competition against fission.

The fission barrier is a key quantity for the existence of SHE. Our results provide the first experimental value for a nucleus with $Z \geq 100$. The extracted barrier of ^{254}No agrees with the value predicted by the macroscopic-microscopic model [4,22], but is smaller than the static barriers of DFT calculations [17,19–21]. These theoretical approaches, which predict different properties of SHE, have discrepant underlying single-particle spectra [46]. The latter partly account for the differences in the fission barrier, where it is dominated by the shell energy. The measured entry distributions show that ^{220}Th and ^{254}No are formed at high spin (up to $20\hbar$) in fusion-evaporation reactions and indicate that high partial waves are dominant in the synthesis of SHE.

This material is based upon work supported by the U.S. Department of Energy, Office of Science, Office of Nuclear Physics, under Contracts No. DE-AC02-06CH11357, No. DE-FG02-91ER-40609, No. DE-FG02-94ER40834, and No. DE-FG02-94ER40848, and by the Labex P2IO. This research used resources of Argonne National Laboratory's ATLAS facility, which is a DOE Office of Science User Facility. We thank H. Esbensen, W. Henning, and P. Möller for helpful discussions.

*Corresponding author.
Present address: Université de Strasbourg, IPHC, 23 rue du Loess, 67037 Strasbourg, France and CNRS, UMR7178, 67037 Strasbourg, France.
ghenning@iphc.cnrs.fr
†Present address: Marshall Space Flight Center, Huntsville, Alabama 35812, USA.

[1] A. J. Sierk, Phys. Rev. C **33**, 2039 (1986).
[2] T. Belgya, O. Bersillon, R. Capote, T. Fukahori, G. Zhigang, S. Goriely, M. Herman, A. Ignatyuk, S. Kailas, A. Koning *et al.*, *Handbook for Calculations of Nuclear Reaction Data, RIPL-2* (IAEA, Vienna, 2006), https://www-nds.iaea.org/RIPL-2/.
[3] Z. Patyk, A. Sobiczewski, P. Armbruster, and K.-H. Schmidt, Nucl. Phys. **A491**, 267 (1989).
[4] P. Möller, A. J. Sierk, T. Ichikawa, A. Iwamoto, R. Bengtsson, H. Uhrenholt, and S. Åberg, Phys. Rev. C **79**, 064304 (2009).
[5] Y. Oganessian, Nucl. Phys. News **23**, 15 (2013).
[6] R. Yanez, W. Loveland, L. Yao, J. S. Barrett, S. Zhu, B. B. Back, T. L. Khoo, M. Alcorta, and M. Albers, Phys. Rev. Lett. **112**, 152702 (2014).
[7] P. Reiter, T. L. Khoo, C. J. Lister, D. Seweryniak, I. Ahmad, M. Alcorta, M. P. Carpenter, J. A. Cizewski, C. N. Davids, G. Gervais *et al.*, Phys. Rev. Lett. **82**, 509 (1999).
[8] M. Leino, H. Kankaanpää, R.-D. Herzberg, A. Chewter, F. Heßberger, Y. Le Coz, F. Becker, P. Butler, J. Cocks, O. Dorvaux *et al.*, Eur. Phys. J. A **6**, 63 (1999).
[9] S. Eeckhaudt, P. Greenlees, N. Amzal, J. Bastin, E. Bouchez, P. Butler, A. Chatillon, K. Eskola, J. Gerl, T. Grahn *et al.*, Eur. Phys. J. A **26**, 227 (2005).
[10] F. Heßberger, S. Antalic, B. Sulignano, D. Ackermann, S. Heinz, S. Hofmann, B. Kindler, J. Khuyagbaatar, I. Kojouharov, P. Kuusiniemi *et al.*, Eur. Phys. J. A **43**, 55 (2010).
[11] R. Clark, K. Gregorich, J. Berryman, M. Ali, J. Allmond, C. Beausang, M. Cromaz, M. Deleplanque, I. Dragojević, J. Dvorak *et al.*, Phys. Lett. B **690**, 19 (2010).
[12] P. Greenlees (private communication).
[13] P. A. Butler, R. D. Humphreys, P. T. Greenlees, R.-D. Herzberg, D. G. Jenkins, G. D. Jones, H. Kankaanpää, H. Kettunen, P. Rahkila, C. Scholey *et al.*, Phys. Rev. Lett. **89**, 202501 (2002).
[14] S. K. Tandel, T. L. Khoo, D. Seweryniak, G. Mukherjee, I. Ahmad, B. Back, R. Blinstrup, M. P. Carpenter, J. Chapman, P. Chowdhury *et al.*, Phys. Rev. Lett. **97**, 082502 (2006).
[15] R.-D. Herzberg, P. T. Greenlees, P. A. Butler, G. D. Jones, M. Venhart, I. G. Darby, S. Eeckhaudt, K. Eskola, T. Grahn, C. Gray-Jones *et al.*, Nature (London) **442**, 896 (2006).
[16] P. Reiter, T. L. Khoo, T. Lauritsen, C. J. Lister, D. Seweryniak, A. A. Sonzogni, I. Ahmad, N. Amzal, P. Bhattacharyya, P. A. Butler *et al.*, Phys. Rev. Lett. **84**, 3542 (2000).
[17] J. L. Egido and L. M. Robledo, Phys. Rev. Lett. **85**, 1198 (2000).
[18] J.-P. Delaroche, M. Girod, H. Goutte, and J. Libert, Nucl. Phys. **A771**, 103 (2006).
[19] L. Bonneau, P. Quentin, and D. Samsoen, Eur. Phys. J. A **21**, 391 (2004).
[20] T. Duguet, P. Bonche, and P.-H. Heenen, Nucl. Phys. **A679**, 427 (2001).
[21] M. Warda and J. L. Egido, Phys. Rev. C **86**, 014322 (2012).
[22] M. Kowal, P. Jachimowicz, and A. Sobiczewski, Phys. Rev. C **82**, 014303 (2010).
[23] B. B. Back, H. C. Britt, O. Hansen, B. Leroux, and J. D. Garrett, Phys. Rev. C **10**, 1948 (1974).
[24] B. B. Back, O. Hansen, H. C. Britt, and J. D. Garrett, Phys. Rev. C **9**, 1924 (1974).
[25] N. Bohr and J. A. Wheeler, Phys. Rev. **56**, 426 (1939).
[26] P. Ring and P. Schuck, *The Nuclear Many-Body Problem* (Springer-Verlag, Berlin, 1980).
[27] I. Lee, Nucl. Phys. **A520**, c641 (1990).
[28] C. Davids, B. Back, K. Bindra, D. Henderson, W. Kutschera, T. Lauritsen, Y. Nagame, P. Sugathan, A. Ramayya, and W. Walters, Nucl. Instrum. Methods Phys. Res., Sect. B **70**, 358 (1992).

[29] H. Gäggeler, D. Jost, A. Türler, P. Armbruster, W. Brüchle, H. Folger, F. Hessberger, S. Hofmann, G. Münzenberg, V. Ninov *et al.*, Nucl. Phys. **A502**, 561 (1989).
[30] M. Itkis, Y. Oganessian, E. Kozulin, N. Kondratiev, L. Krupa, I. Pokrovsky, A. Polyakov, V. Ponomarenko, E. Prokhorova, B. Pustylnik *et al.*, Il Nuovo Cimento A **111**, 783 (1998).
[31] Y. T. Oganessian, V. K. Utyonkov, Y. V. Lobanov, F. S. Abdullin, A. N. Polyakov, I. V. Shirokovsky, Y. S. Tsyganov, A. N. Mezentsev, S. Iliev, V. G. Subbotin *et al.*, Phys. Rev. C **64**, 054606 (2001).
[32] P. Benet, Ph.D. thesis, Université Louis Pasteur de Strasbourg, 1988.
[33] M. Jääskeläinen, D. Sarantites, R. Woodward, F. Dilmanian, J. Hood, R. Jääskeläinen, D. Hensley, M. Halbert, and J. Barker, Nucl. Instrum. Methods Phys. Res., **204**, 385 (1983).
[34] G. Henning, Ph.D. thesis, Université Paris Sud, 2012.
[35] J. Allison, K. Amako, J. Apostolakis, H. Araujo, P. Dubois, M. Asai, G. Barrand, R. Capra, S. Chauvie, R. Chytracek *et al.*, IEEE Trans. Nucl. Sci. **53**, 270 (2006).
[36] S. Agostinelli, J. Allison, K. Amako, J. Apostolakis, H. Araujo, P. Arce, M. Asai, D. Axen, S. Banerjee, G. Barrand *et al.*, Nucl. Instrum. Methods Phys. Res., Sect. A **506**, 250 (2003).
[37] W. Reviol, C. J. Chiara, M. Montero, D. G. Sarantites, O. L. Pechenaya, M. P. Carpenter, R. V. F. Janssens, T. L. Khoo, T. Lauritsen, C. J. Lister *et al.*, Phys. Rev. C **74**, 044305 (2006).
[38] A. Marchix, Ph.D. thesis, Université de Caen/Basse-Normandie, 2007.
[39] V. I. Zagrebaev, A. V. Karpov, A. S. Denikin, and A. P. Alekseev, NRV code, http://nrv.jinr.ru/nrv/.
[40] L. G. Moretto, L. Phair, and G. J. Wozniak, Phys. Rev. C **67**, 017301 (2003).
[41] P. Möller and R. MacFarlane, Fission Potential-Energy Surfaces Calculated Versus ϵ_2 and γ, http://t2.lanl.gov/nis/data/astro/molnix96/peseps2gamma-fis.html.
[42] A. Heinz, T. Khoo, P. Reiter, I. Ahmad, P. Bhattacharyya, J. Caggiano, M. Carpenter, J. Cizewski, C. Davids, W. Henning *et al.*, Nucl. Phys. **A682**, 458 (2001).
[43] P. Moller, J. Nix, W. Myers, and W. Swiatecki, At. Data Nucl. Data Tables **59**, 185 (1995).
[44] P. Moller, J. Nix, W. Myers, and W. Swiatecki, Nuclear Ground-State Masses and Deformations, http://t2.lanl.gov/nis/data/astro/molnix96/massd.html.
[45] S. Bjørnholm and J. E. Lynn, Rev. Mod. Phys. **52**, 725 (1980).
[46] D. Seweryniak, T. Khoo, I. Ahmad, F. Kondev, A. Robinson, S. Tandel, M. Asai, B. Back, M. Carpenter, P. Chowdhury *et al.*, Nucl. Phys. **A834**, 357c (2010); The 10th International Conference on Nucleus-Nucleus Collisions (NN2009), http://www.sciencedirect.com/science/article/pii/S0375947410000400.